Energy & Buildings 256 (2022) 111700

Contents lists available at ScienceDirect

Energy & Buildings

journal homepage: www.elsevier.com/locate/enb

Techno-economic analysis of metal-hydride energy storage to enable year-round load-shifting for residential heat pumps

Patrick Krane, Davide Ziviani, James E. Braun, Neera Jain, Amy Marconnet *

School of Mechanical Engineering, Purdue University, West Lafayette, IN, United States

ARTICLE INFO

Article history:
Received 6 September 2021
Revised 29 October 2021
Accepted 18 November 2021
Available online 27 November 2021

Keywords:
Thermal Energy Storage
Metal Hydrides
Residential HVAC systems
Year-round Energy Storage

ABSTRACT

Thermal energy storage (TES), such as ice storage, is often used with air conditioning systems to shift cooling loads away from peak hours, reducing operating costs if time-of-use electricity rates are available. Phase change materials (PCMs) have been investigated for energy storage with heating systems; however, a single PCM cannot be used for storage with both cooling and heating since PCMs have fixed phase-change temperatures. Thermochemical energy storage with metal hydrides can be used for this purpose since the reaction used to store energy depends on both temperature and pressure, allowing for variable-temperature storage. In this paper, we propose a novel TES system design using metal hydrides coupled to a heat pump for residential heating and cooling and present a system model. The model is used to analyze system performance and predict cost savings for year-round use in a residential building. This system is shown to be capable of shifting heating and cooling loads, but only achieves cost savings of $13/year at existing utility rates. The payback period of the system exceeds 35 years across a range of rates more favorable to energy storage, primarily due to the high cost of metal hydrides. Potential improvements to the system are discussed.

1. Introduction

Time-of-use (TOU) rates for electricity, in which electricity costs vary between more expensive 'on-peak' periods and less expensive 'off-peak' periods, are widely available for commercial buildings and in recent years have become more widely available for residential buildings. Consequently, thermal energy storage systems can be used to reduce operating costs by shifting heating or cooling loads from on-peak to off-peak hours [1,2]. If the same energy storage system could be used for both heating and cooling, it could achieve higher cost savings without the increased initial cost for using different systems for heating and cooling.

Thermal energy storage can be categorized as either sensible heat storage, latent heat storage, or thermochemical storage [2,3]. Sensible heat storage (storing heat by changing the temperature of the storage material) can be used for both heat storage and cold storage [4], but it has the disadvantage that it has a significantly lower energy density than either latent heat or thermochemical energy storage [3,5]. Latent heat storage (storing heat through a phase change) can be used for storage for both heating and cooling, but only through the use of two separate phase-change material (PCM) storage systems [6]. The same PCM cannot be used since a PCM used for heat storage must have a phase-change temperature above room temperature, while a PCM for cool storage must have one below room temperature. Since the phase-change temperature of a PCM can currently only be varied a few degrees (requiring substantial energy costs) [7], it is not currently feasible to use the same material for both heat storage and cold storage. Thermochemical energy storage (storing heat through a chemical reaction) has the potential to enable high energy–density TES for both heating and cooling because it does not operate at a fixed phase change temperature. This is because the reactions used to store and release heat depend on both the temperature and concentration of the reactants [3].

One type of thermochemical storage material that could potentially be used for both heating and cooling is metal hydrides. Metal hydrides are metal alloys that adsorb and desorb hydrogen through exothermic and endothermic reactions, respectively. Whether this reaction occurs depends on both temperature and pressure, which means that the temperature at which energy is stored and released by metal hydrides can be changed by changing the pressure [8,9]. This allows metal hydrides to be used for variable-temperature energy storage

In this paper, we perform an initial feasibility study of a two-reactor metal hydride energy storage system integrated with a

* Corresponding author.
E-mail address: marconnet@purdue.edu (A. Marconnet).

https://doi.org/10.1016/j.enbuild.2021.111700
0378-7788/

Nomenclature

Variables (Units)

A_s	Surface Area (m^2)
c	Specific Heat (J/(kg*K))
C_A	Arrhenius Pre-Exponential Factor (1/s)
COP	Coefficient of Performance
c_P	Constant-Pressure Specific Heat (J/(kg*K))
E_A	Reaction Activation Energy (J/kg)
$\dot{g}$	Internal Heat Generation (W)
GHI	Global Horizontal Irradiance (W/m^2)
h	Specific Enthalpy (J/kg)
h_{conv}	Convection Heat Transfer Coefficient (W/m^2)
k_r	Heat Ratio
m	Mass (kg)
$\dot{m}$	Mass Flow Rate (kg/s)
P	Pressure (Pa)
$\dot{Q}$	Heat Transfer Rate (W)
r	Reaction Rate ($\frac{dw}{dt}$) (kg H / (kg M * s))
R	Gas Constant (J/(kg*K))
T	Temperature (K)
UA	Overall Heat Transfer Coefficient (W/K)
V	Volume (m^3)
w	Weight Fraction (kg H / kg M)
$\dot{W}$	Power (W)
ΔH	Enthalpy of Reaction (J / kg M)
ε	Effectiveness
η_s	Isentropic Efficiency
θ_b	Solar Cooling Factor (K)
φ	Porosity

Subscripts

A	$MmNi_{4.5}Cr_{0.5}$ Reactor
B	$LaNi_5$ Reactor
comp	Compressor
design load	Design Load
eq	Equilibrium
elec	Electric heating
ground	Ground Heat Exchanger
H	Hydrogen
house	House
hp	Heat Pump
hyd	Hydride
in	Inlet
indoor	Indoor Loop
load	Load
M	Metal
max	Maximum
off	Off-peak
on	On-peak
out	Outlet
outdoor	Outdoor Loop
r	Reactor
s	Isentropic
setpoint	Setpoint
solar	Solar
tar	Target
wg	Water Glycol

vapor-compression heat pump for heating and cooling. The two-reactor design is used instead of a single-reactor system because in the latter, the released hydrogen is compressed and stored in a high-pressure tank which was considered a safety concern in a residential setting. This system is a unique TES system for heating and cooling in residential buildings that can be used year-round to reduce operating costs with TOU electricity rates. The system analyzed is a variable-temperature system (a dynamic model of the hydride reactors is used, with temperature as one of the state variables) but the optimization of the hydride operating temperatures is beyond the scope of this paper. This feasibility study demonstrates a potential system design and control logic that can be used for metal hydride energy storage (described in Section 1), and then describes the performance of this system when used for a residential building, including estimating payback periods for installing this system to evaluate economic viability (Section 4). Conclusions are presented in Section 5.

2. Literature review

2.1. Thermal energy storage for building heating and cooling

Ice storage is the most commonly-used thermal storage technology for load shifting with air conditioning (A/C) systems in commercial buildings [10,11]. There have been numerous studies evaluating the effect of ice storage systems on building operating costs and energy usage [12–14] and examining the optimal control logic for load-shifting [15,16]. Ice storage has been found to be effective at reducing operating costs for different TOU rates and locations [1,13,14]. While less commonly used than ice storage due to its lower energy density [1], sensible heat storage using chilled water has also been studied and implemented in commercial buildings [11,17,18]. Other phase-change materials (PCMs) have been considered as alternatives to ice storage, primarily because the low phase-change temperature of ice leads to reduced performance when charging the system, but none have achieved the large-scale commercial application ice storage has [1,2,19]. Recent work has examined the extension of ice storage to residential buildings, and concluded that it could be economically viable only in warm climates with a long cooling season [20]. This conclusion indicates that energy storage might be viable in a wider range of locations if it could be used year-round, for both cooling and heating systems.

Albeit not as commonly used as energy storage for cooling in buildings, both sensible heat and latent heat storage for heating in buildings have been previously considered [2,5,21,22]. Water is the most commonly-studied material for sensible heat storage (as it is for sensible cold storage) [4,22,23]. Materials such as paraffin wax [6,21,24] and salt hydrates [21,22] as PCMs for latent-heat storage for building heating have also been studied. While a single PCM cannot normally be used year-round, this can be done for systems with district heating and an absorption chiller, since in the summer the storage system can be discharged as a heat source for the absorption chiller [25,26] and in the winter used for heat storage. However, this is not applicable for an electrically-driven vapor-compression system that provides heating and cooling, which requires the use of separate cold storage in cooling mode and heat storage in heating mode.

Thermochemical energy storage has also been studied for short-term energy storage for heating and cooling, similar to latent heat and sensible heat storage [3,27]. In addition, because thermochemical energy storage does not have a fixed phase-change temperature, it has been studied for long-term seasonal energy storage, since the energy does not have to be stored at a temperature differ-

ent from the environment [3,27,28]. However, even for short-term storage, thermochemical energy storage has the potential to allow for the same storage system to operate at different temperatures in different climates, to adjust the operating temperature if needed during operation, and potentially to use the same storage system for both heating and cooling. This potential of thermochemical energy storage has not received much attention, with most systems previously considered being intended specifically for heating or cooling [29], except those that are used with district heating and an absorption chiller in a manner similar to the latent-heat systems described above [27].

2.2. Metal hydrides

The material property that determines whether a metal hydride will react with hydrogen is the equilibrium pressure. The equilibrium pressure is a function of both the hydride temperature and the weight fraction of hydrogen stored in the hydride [8,9]. Equilibrium pressure has different values for absorption and desorption [9]. If the hydrogen pressure surrounding the hydride is lower than the equilibrium pressure for desorption, hydrogen is desorbed; if the pressure is greater than the equilibrium pressure for absorption, hydrogen is adsorbed. No reaction occurs in the pressure is between the equilibrium pressure values for absorption and desorption.

While they have not previously been examined for use with a building HVAC system, metal hydrides have previously been considered for use in a variety of systems, including hydrogen storage for fuel cells [30,31], heat pumps for air conditioning and refrigeration systems [32–36], and energy storage for concentrated solar power [37–40]. Both metal hydride heat pumps and energy storage systems typically use a pair of metal hydride reactors that allow transfer of hydrogen from one to the other, with one reactor used to store and release energy through the adsorption and desorption reactions and the other reactor used to store the hydrogen released by the first reactor. Metal hydride systems can be characterized as temperature-driven or pressure-driven systems. In a temperature-driven system, the flow between hydride reactors is driven by a difference in the equilibrium pressures of the reactors [33–38,40] that depends on their temperatures, which are controlled through heat transfer to and from the reactors. A temperature-driven system requires four metal hydride reactors for a heat pump (so that one pair is providing the load while the other is being charged) [33–36] and two reactors for energy storage (since energy storage does not have to provide a continuous load) [37,38,40]. A pressure-driven metal hydride heat pump uses a compressor to drive hydrogen flow between reactors, thereby adjusting the pressures in the reactors away from equilibrium and driving the reactions [32,35]. Pressure-driven systems have been found to achieve a higher coefficient of performance (COP) than temperature-driven systems [35] but require the increased cost of installing and running a compressor, while temperature-driven systems have the advantage of being driven using waste heat. For a pressure-driven energy storage system, a pressure vessel is used to store hydrogen instead of a second hydride reactor [38,39], which has the advantage of reducing the initial cost of the system, but the disadvantages of requiring a larger storage volume and requiring increased operating costs for hydrogen compression [38].

3. Model description

In this study, we describe a potential system architecture for a metal hydride TES system used with residential heating and cooling and a model of this system that can be used to calculate the effect this system has on building energy usage and operating costs. The calculated energy usage and operating costs will be used to evaluate the viability of this system design. The system architecture described is a novel design for this application, since it is to our knowledge the first to use metal hydrides for TES with a residential heating and cooling system. The system modelled is a high energy density, variable-temperature system that is used with both building heating and cooling.

3.1. System architecture

The focus of this study is a two-reactor metal hydride system. Each reactor is assumed to be a shell-and-tube heat exchanger in which the shell is filled with a metal hydride (referred to as the "metal hydride bed") and the tubes enable heat transfer between the metal hydride bed and a circulating fluid. When operating, the two hydride reactors are connected, and one metal hydride reactor stores the hydrogen released by the other. The process of releasing hydrogen is endothermic, while the process of absorbing it is exothermic. The operation of this system for cooling mode is shown in Fig. 1, and the operation for heating mode is shown in Fig. 2. The system could be used for residential or commercial buildings, but in this study is only evaluated for a residential application. At the center of the system is a packaged propane heat pump with a 4-way valve that is connected to two water-glycol loops. These two water-glycol loops are an *indoor loop*, which exchanges heat with an indoor heat exchanger in the house as well as the heat pump, and an *outdoor loop*, which exchanges heat with an external heat exchanger as well as the heat pump. The 4-way valve within the heat pump cycle is employed to switch between heating and cooling modes by reversing which loop the heat pump transfers heat to and which it removes heat from. In addition to these components, there are the two metal hydride reactors which are connected to allow hydrogen to flow between them.

A compressor on the hydrogen line can be used to drive hydrogen flow between these reactors, with valves configured such that it can drive flow in either direction. The reactors are charged and discharged by exchanging heat with their respective water-glycol flow stream. Flow can be diverted from either water-glycol loop to exchange heat with either metal hydride reactor. The reactors are labeled low-temperature and high-temperature because the hydrides in them are chosen to have a relationship between equilibrium pressure and temperature that will maximize how much flow will be temperature-driven. Thus, one reactor is at a lower temperature than the other. It should be noted that low-temperature and high-temperature are used here as relative terms: neither reactor will ever be colder than approximately −20 °C or warmer than approximately 50 °C.

Ultimately, the system operates in 6 modes: conventional heating or cooling mode with no interaction with the thermal energy storage system, charging during heating or cooling, and discharging during heating or cooling. The system operation in charging and discharging modes when cooling the house can be seen in Fig. 1. In cooling mode, the evaporator in the heat pump provides the cooling load that will be delivered by the indoor loop, while the condenser heats the water glycol in the outdoor loop, which is restored to its original temperature by exchanging heat with the external heat exchanger. In charging mode, the outdoor loop heats the high-temperature reactor (metal hydride bed); this, as well as the compressor if necessary, drives a desorption reaction that releases hydrogen to flow to the low-temperature reactor, which absorbs the hydrogen and releases heat to the indoor loop. Then, in discharging mode, flow from the outdoor loop is diverted at a different location (as seen in Fig. 1, water glycol flows to the reactor from the heat pump when charging but from the external unit when discharging), where it is at a lower temperature, while

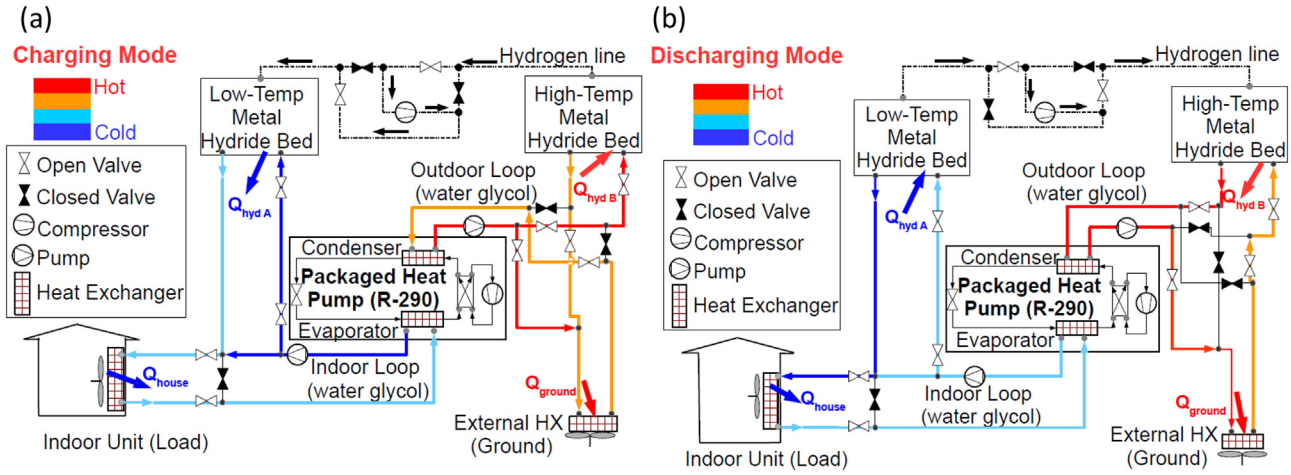

Fig. 1. (a) Cooling system in charging mode. Flow is diverted from the outdoor loop to heat the high-temperature reactor (metal hydride bed); this, as well as the compressor if needed, drives the hydride to release hydrogen that flows to the low-temperature reactor, which absorbs the hydrogen and releases heat to the indoor loop. (b) Cooling system in discharge mode. Flow from the outdoor loop to the high-temperature reactor is now at a lower temperature than in charging mode. This, and the compressor, if needed, drives hydrogen from the low-temperature reactor back to the high-temperature reactor. As the low-temperature reactor releases hydrogen, it absorbs heat from the indoor loop, cooling the water glycol before it returns to the house and thus reducing the load on the heat pump. For ease of viewing, additional piping used only in heating mode is not shown in either image.

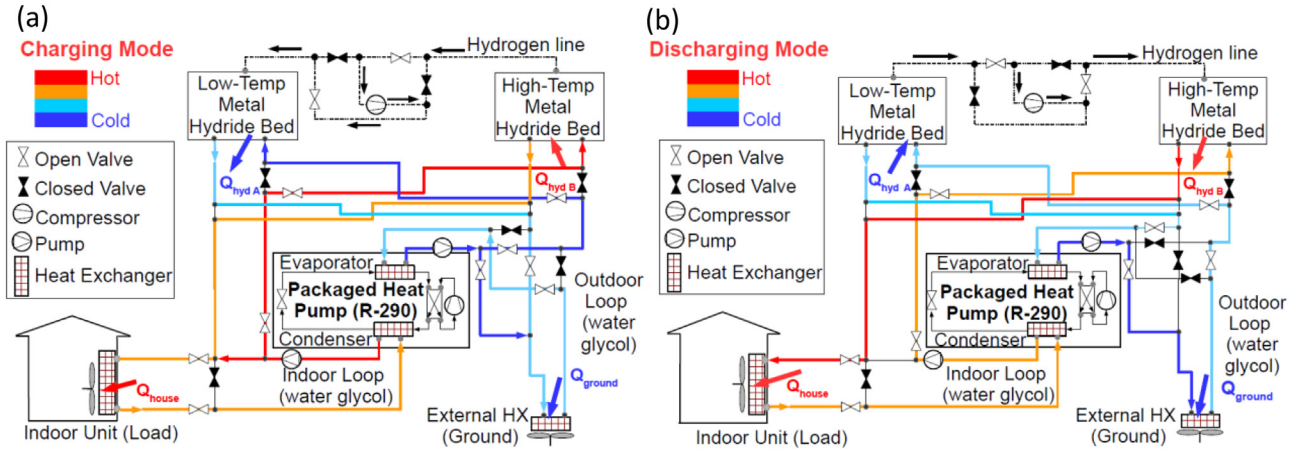

Fig. 2. (a) Heating system in charging mode. Flow is diverted from the indoor loop to heat the high-temperature reactor; this, as well as the compressor if needed, drives the hydride to release hydrogen that flows to the low-temperature reactor, which absorbs the hydrogen and releases heat to the outdoor loop. (b) Heating system in discharge mode. Flow from the indoor loop to the high-temperature reactor is now at a lower temperature than in charging mode, and it is now heated by the high-temperature reactor, which thus delivers a portion of the heating load. This, and the compressor, if needed, drives hydrogen from the low-temperature reactor back to the high-temperature reactor. As the low-temperature reactor releases hydrogen, it absorbs heat from the outdoor loop.

the low-temperature reactor now desorbs hydrogen and absorbs heat from the indoor loop. The change in the temperature of the high-temperature reactor changes the equilibrium pressure, so that the hydrogen desorbed by the low-temperature reactor now flows back to the high-temperature reactor (with this flow driven by the compressor if the change in equilibrium pressure is insufficient), which absorbs it and releases heat to the outdoor loop. Since the low-temperature reactor transfers heat to the indoor loop when charging and absorbs heat from it when discharging, the metal hydride energy storage system can be used to shift a portion of the load from on-peak hours to off-peak.

As shown in Fig. 2, the system is charged and discharged in heating mode in an analogous way as cooling mode, except for switching the connection of the water-glycol loop to the metal hydride reactors. In other words, the indoor loop heats the high-temperature reactor in charging mode and receives heat from it in discharging mode. As in cooling mode, the temperature of the flow diverted from the outdoor and indoor loops and the compressor are used to drive the absorption and desorption reactions and the flow of hydrogen between the reactors. Compared to a conventional heat pump system, the heat pump has an increased heating load during charging and a decreased load during discharging enabling a load shift from on-peak to off-peak hours.

3.2. System model

A diagram of the system model can be seen in Fig. 3. This model consists of two main sub-models: one for the secondary (indoor and outdoor) loops and one for the metal hydride reactors. External conditions are used to determine the load on the building (Section 3.2.1), which is then used as an input for the secondary loop model. The secondary loop model (Section 3.2.2) is solved iteratively to find a solution that satisfies the requirements for both the heat pump and the secondary loops, then uses a heat pump performance map to calculate the power required by the heat

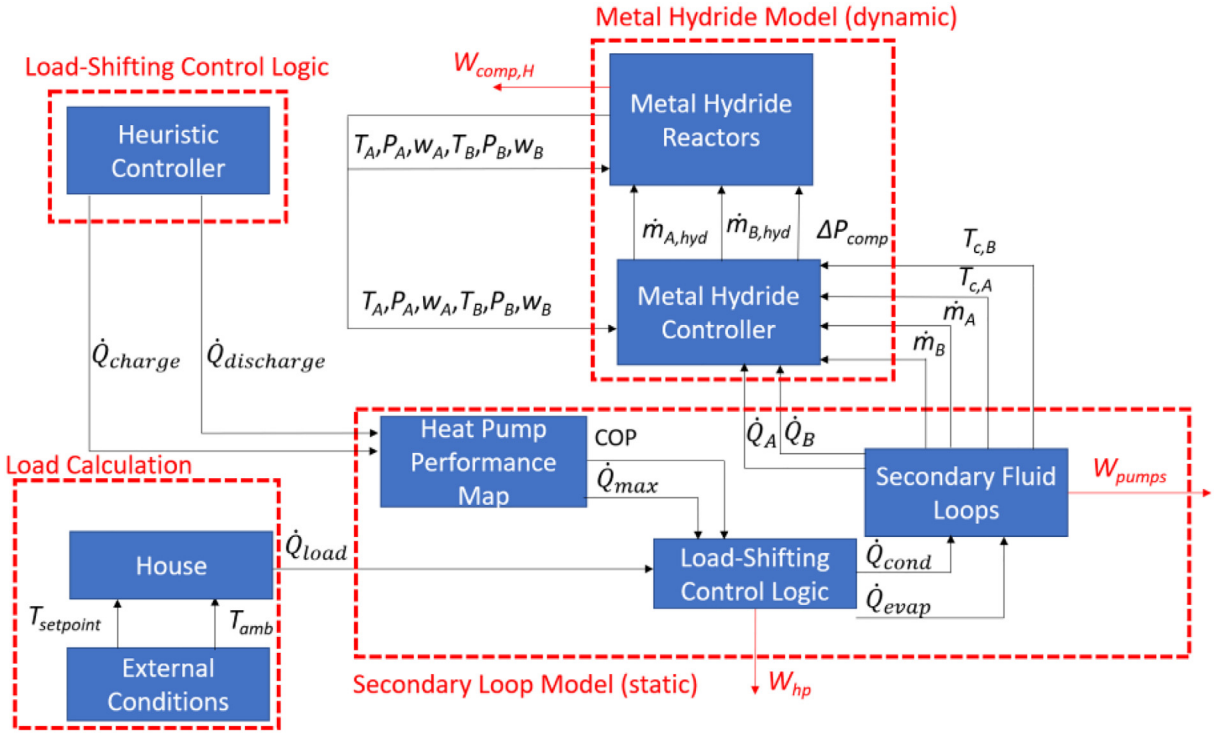

Fig. 3. Diagram of the complete system model. External conditions are used to determine the load on the building, which is an input for the secondary loop model. The secondary loop model is solved iteratively to find a solution that satisfies the requirements for both the heat pump and the secondary loops. Then, the calculated heat transfer rates, indoor and outdoor loop mass flow rates, and fluid inlet temperatures are used by the controller to solve for the control inputs to the metal hydride reactors, which are used to calculate the updated reactor state.

pump. Then, the calculated heat transfer rates, indoor and outdoor loop mass flow rates, and fluid inlet temperatures are used by an embedded controller to solve for the control inputs to the metal hydride reactors, which are used to calculate the updated reactor state (Section 3.2.3). The target heat rates for the hydride reactors are determined by the load-shifting control logic (Section 3.2.4), which determines when to charge and discharge the storage system.

3.2.1. Load calculations

The heating or cooling load at the house is calculated using a simple model that employs a quasi-steady-state assumption. This model calculates the load using an overall *UA*-value determined assuming that a cooling load of 3 RT (10.55 kW) is needed to maintain a setpoint temperature of 72°F (22.2 °C) at an outdoor temperature of T_∞ = 95°F (35 °C) from

$$\dot{Q}_{designload,house} = UA\left(T_{setpoint} - T_\infty + \theta_b\right) + \dot{g}, \tag{1}$$

where $\dot{g}$ is the internal gain, $T_{setpoint}$ is the desired temperature inside the home, and θ_b is a correction factor for heating by solar radiation. It is further assumed that this design cooling load occurs when solar irradiation is at its maximum, and the internal gain is the average of its value across the entire time period used in the study (e.g., a year).

In estimating the overall *UA* using Eq. (1), the design solar temperature effect, θ_b, is assumed to be 8.2°F (4.6 °C) based on the ASHRAE recommendations for an unshaded wall [41]; a real house will have higher irradiation through the windows and lower irradiation on the unshaded walls, so this value was chosen as an intermediate value. The internal gain, $\dot{g}$, is assumed to be equal to the average electric power consumed by the house excluding the HVAC system. Data for electric power consumption is taken from data for typical residential hourly electric loads from the Office of Energy Efficiency & Renewable Energy [42]; for estimating the value of *UA*, the average value for the time period studied is used. The heat gain rate due to solar radiation at the conditions used to calculate the design load is calculated with

$$\dot{Q}_{solar,max} = \dot{Q}_{designload,house} - \left[UA\left(T_{setpoint} - T_\infty\right) + \dot{g}\right] = UA \cdot \theta_b. \tag{2}$$

A simple model of solar heating effects is used in which the maximum solar heating effect is linearly scaled at each time step, according to the ratio of the horizontal irradiance for the time step to the maximum value for the year. This is given by

$$\dot{Q}_{solar} = \frac{GHI}{GHI_{max}}\dot{Q}_{solar,max}, \tag{3}$$

where *GHI* is the average global horizontal irradiance for the time step and GHI_{max} is the maximum value of *GHI* in the weather data for a given location.

The house heating or cooling load for any time step, $Q_{load,\ house}$, is calculated using Eq. (4), with the values of $T_{setpoint}$, $\dot{g}$, and Q_{solar} determined using location-specific data:

$$\dot{Q}_{load,house} = UA\left(T_{setpoint} - T_\infty\right) + \dot{g} + \dot{Q}_{solar}. \tag{4}$$

For cooling, the setpoint is designated as 72°F (22.2 °C) at all times except between 9 AM and 5 PM on weekdays, when it is 76°F (24.4 °C). During heating, it is set to 68°F (20 °C), and lowered to 64°F (17.8 °C) from 9 AM to 5 PM on weekdays. It is assumed that the system is only turned on for outdoor temperatures either 5°F (2.78 °C) greater or 15°F (8.33 °C) less than the setpoint.

3.2.2. Secondary loops model

In each secondary loop, the temperature of the water-glycol mixture changes in the following locations that are depicted in Fig. 4: (1) where it exchanges heat with the heat pump, (2) where it exchanges heat with a hydride reactor, and (3) where it

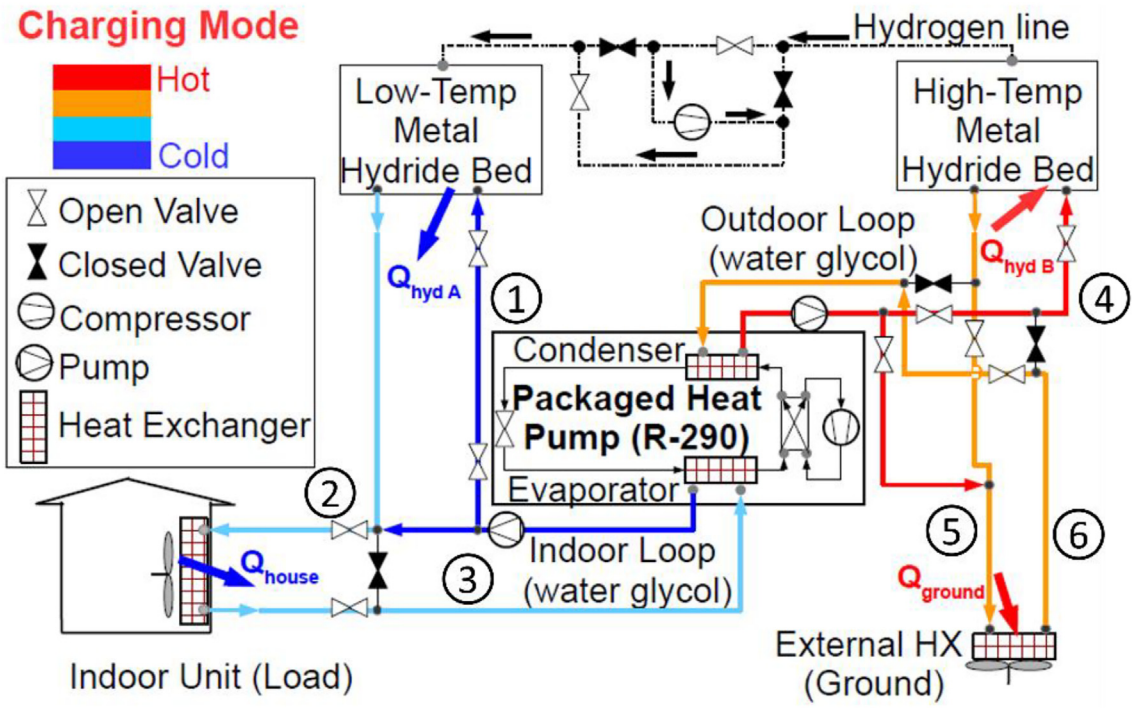

Fig. 4. Diagram of the system in cooling charge mode with labels for the different points used in the secondary loops calculations.

exchanges heat with either the indoor heat exchanger or the external heat exchanger. Since the fluid in each loop is heated or cooled at three different points, there are six different points where the temperature of the fluid must be solved for, labelled (1)-(6) in Fig. 4. The change in the water-glycol temperature as it flows through each pump is neglected, but the change in pressure is estimated in order to calculate the pumping work required by the system. Thus, calculating the thermodynamic state of the system requires solving for 6 temperatures, 6 heat transfer rates (one at each component), and 4 mass flow rates (the flow rate in the indoor and outdoor loops and the flow rate diverted to a reactor from each loop). The heat transfer rate from the indoor heat exchanger to the indoor loop, $\dot{Q}_{house}$, is known for given outdoor and setpoint temperatures. Load-shifting strategies (described in Section 3.2.4) specify the ratio between the heat transfer rate from the hydride bed to the indoor loop, $\dot{Q}_{hyd,indoor}$, and the heat transfer rate from the heat pump to the inner loop, $\dot{Q}_{hp,indoor}$. Given the supply temperatures to the heat pump, the COP and capacity of the heat pump can be calculated from the heat pump maps for a scroll compressor described in Appendix A [43]. Thus, the heat transfer rate from the heat pump to the outside loop, $\dot{Q}_{hp,outdoor}$, can be determined from the COP. Furthermore, to better control the hydride reactions, the ratio between the heat transfer rates in the two hydride reactors is set to a constant, k_r. As discussed in our previous work [44], the value for this ratio should be one that allows the reactors to operate predominantly in a near-equilibrium state, in order to avoid saturation of the control variables used to maintain these heat rates (discussed in Section 2.7). The values for k_r that were found to best achieve this were $k_r = 0.85$ in charging mode and $k_r = 0.75$ in discharging mode.

The equations for heat transfer rates, when combined with energy balances performed on each of the 6 components, results in 10 equations. Nine of these equations are summarized in Equations 5–10 (the tenth is $\dot{Q}_{hp,indoor}$ being set by the load-shifting control logic shown in Fig. 7):

$$\dot{Q}_{hp,indoor} = \dot{m}_{wg,indoor} c_{wg} (T_1 - T_3) \tag{5}$$

$$\dot{Q}_{hyd,indoor} = \dot{m}_{wg,indoor} c_{wg} (T_2 - T_1) \tag{6}$$

$$\dot{Q}_{house} = \dot{m}_{wg,indoor} c_{wg} (T_3 - T_2) = \begin{cases} -\dot{Q}_{load,house}, & cooling \\ -\left(\dot{Q}_{load,house} - \dot{Q}_{elec}\right), & heating \end{cases} \tag{7}$$

$$\dot{Q}_{hp,outdoor} = \dot{m}_{wg,outdoor} c_{wg} (T_4 - T_6) = \begin{cases} 1 + \frac{1}{COP}\dot{Q}_{hp,indoor}, & cooling \\ 1 - \frac{1}{COP}\dot{Q}_{hp,indoor}, & heating \end{cases} \tag{8}$$

$$\dot{Q}_{hyd,outdoor} = \dot{m}_{wg,outdoor} c_{wg} (T_5 - T_4) = -k_r \dot{Q}_{hyd,indoor} \tag{9}$$

$$\dot{Q}_{ground} = \dot{m}_{wg,outdoor} c_{wg} (T_6 - T_5) \tag{10}$$

In these equations, $\dot{m}_{wg,indoor}$ is the indoor loop flow rate, $\dot{m}_{wg,outdoor}$ the outdoor loop flow rate, c_{wg} is the specific heat of the water glycol, T_n the temperature of the water glycol at location n shown in Fig. 4 for $n = 1$ to 6, $\dot{Q}_{hp,indoor}$, $\dot{Q}_{hyd,indoor}$, and $\dot{Q}_{house}$, are the heat transfer rates to the water glycol in the indoor loop from the heat pump, hydride reactor, and indoor heat exchanger, respectively, and $\dot{Q}_{hp,indoor}$, $\dot{Q}_{hyd,out}$, and $\dot{Q}_{ground}$ are the heat transfer rates to the water glycol in the outdoor loop from the heat pump, hydride reactor, and external heat exchanger, respectively. Q_{elec} is the heat transfer rate to the house from auxiliary electric heating, which is used if the heating load at the house is greater than what can be met by the heat pump. The equations above are used for charging mode; for discharging mode, Eqs. 5–8 are still used, but since flow in the outdoor loop now moves from the external unit to the hydride reactor rather than the other way around, the last two equations are

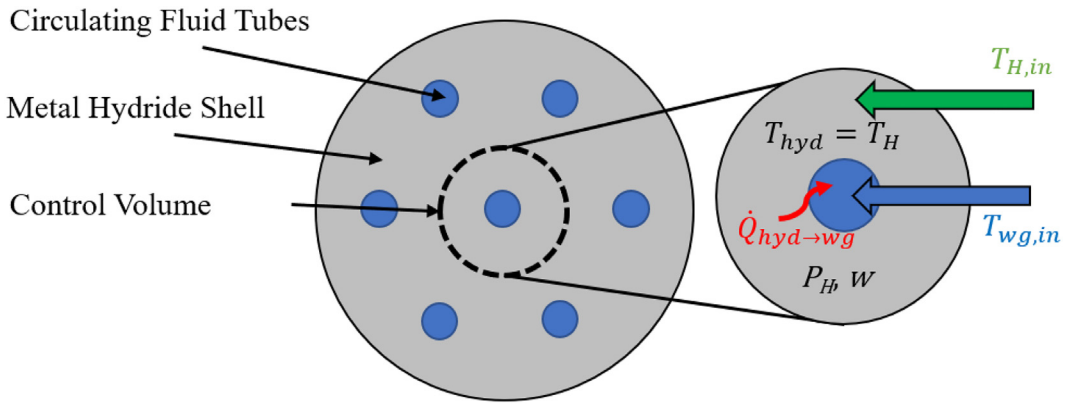

Fig. 5. Diagram of the metal hydride subsystem model showing the control volume in each shell-and-tube reactor.

$$\dot{Q}_{ground} = \dot{m}_{wg,outdoor} c_{wg} (T_5 - T_4) \tag{11}$$

and

$$\dot{Q}_{hyd,outdoor} = \dot{m}_{wg,outdoor} c_{wg} (T_6 - T_5) = -k_r \dot{Q}_{hyd,indoor}. \tag{12}$$

Since the controller for the hydride reactor determines the mass flow rate of water glycol, $\dot{m}_{wg,r}$, sent to each reactor, there are 12 equations and 16 unknowns. Therefore, four variables must be specified to solve the system of equations. To avoid physically unrealistic operating temperatures, the outlet temperature at the house (T_3) is specified based on the indoor temperature, to ensure that flow leaves the house colder than room temperature in cooling mode and hotter than room temperature in heating mode. Similarly, the outlet temperature at the external heat exchanger (T_6 in charge mode, T_5 in discharge) is defined based on the ambient temperature, to ensure that flow leaves the external heat exchanger at a temperature above ambient temperature in cooling mode and below ambient temperature in heating mode. In addition to these temperatures, the inlet temperatures of the hydride reactors are also defined in each case. Within the constraints imposed by the other defined temperature values, the values used for the hydride reactor inlet temperatures are selected based on the temperature–pressure relations, so that the resulting operating pressures will allow for temperature-driven flow in most cases while staying within the desired limits of hydrogen pressure. Since water glycol flows from the external heat exchanger to the hydride reactor in the outdoor loop during discharge mode, the inlet of the outdoor hydride reactor and the outlet of the external heat exchanger are both position 5. Thus, temperature must be defined in another position as well, so the outlet temperature of the hydride reactor is also defined. This temperature is defined because it is also the inlet temperature to the heat pump, and thus used in calculating COP. Thus, T_1, T_3, and T_6 are always specified while T_4 is defined only if charging and T_5 only if discharging. The algorithm used to determine the values which are fixed for these temperatures is given in Appendix B. At each time step, the pump work is calculated from the water-glycol mass flow rate, the heat pump work is calculated using the COP and heat transfer from the heat pump, and the hydrogen compressor work is calculated from the mass flow rate of hydrogen and pressure difference across the compressor (described in Section 3.2.3). These work terms, as well as electric heating work (determined based on the control logic explained in Section 3.2.4) and an estimated value for typical non-HVAC work at a given time, are used to calculate the cost of electricity at each time step.

3.2.3. Hydride reactor model

A subsystem model of the metal hydride reactors determines the operating temperatures and pressures, the rate of change of the hydrogen in each reactor, and the heat transfer with the water glycol flowing through a given secondary loop. This subsystem model consists of the two shell-and-tube heat exchangers used as metal hydride reactors. A diagram of this heat exchanger is shown in Fig. 5. As shown in this figure, in each unit cell there is hydrogen flow into or out of the shell, water glycol flow in the tube, and heat transfer between the water glycol and the metal hydride. The heat exchanger model considers a single water-glycol tube and the surrounding metal hydride as a representative unit cell control volume and assumes, by symmetry, that these unit cell results can be used for the reactor as a whole. The materials selected for use as the hydrides in the reactors are $LaNi_5$ in the high-temperature reactor and $MmNi_{4.5}Cr_{0.5}$ in the low-temperature reactor. These materials were selected to minimize compressor work by choosing materials such that, in both heating and cooling modes, as much hydrogen flow as possible can be driven by the difference in equilibrium pressures at their operating temperatures rather than by compressor work. Key properties of these materials are described in Table 1. The material properties of these metal hydrides are taken from a MATLAB Toolbox developed by Voskuilen, Waters, and Pourpoint [9].

For each tank, the energy balance is given by

$$\left(m_{hyd} c_{hyd} + m_H c_{p,H}\right) \frac{dT_r}{dt} = r m_{hyd} \Delta H + \varepsilon \dot{m}_{wg} c_{wg} \left(T_{wg,in} - T_r\right) + \dot{m}_{H,in} c_{p,H} \left(T_{H,in} - T_r\right). \tag{13}$$

In these equations, m_H is the hydrogen mass, m_{hyd} is the hydride mass, $c_{p,H}$ is the hydrogen specific heat, c_{hyd} is the hydride specific heat, r is the reaction rate, ΔH is the enthalpy of reaction, ε is the effectiveness of the heat exchanger, $\dot{m}_{wg}$ is the water-glycol mass flow rate through the reactor, T_r is the temperature in the hydride bed, $T_{wg,in}$ is the inlet water-glycol temperature, $\dot{m}_{H,in}$ is the hydrogen flow rate into the reactor, and $T_{H,in}$ is the hydrogen inlet temperature.

A governing equation for pressure is determined using a mass balance equation that relates the evolution of the hydrogen mass to the reaction rate and the flow rate of hydrogen, $\dot{m}_H$ (note that unlike $\dot{m}_{H,in}$, $\dot{m}_H$ is used for flow into and out of the reactor), then converting from mass to pressure using the ideal gas law:

$$\frac{dP_H}{dt} = \frac{RT}{\varphi V} \frac{dm_H}{dt} = \frac{RT}{\varphi V} \left(r m_{hyd} + \dot{m}_H \right). \tag{14}$$

In this equation, R is the gas constant for hydrogen, ϕ is the porosity of the hydride bed, and V is the volume of the hydride bed.

Table 1
Material properties, including maximum weight fraction (w_{max}) and enthalpy of reaction (ΔH), for the metal hydrides selected as the preliminary materials for the system [9].

		Absorption			Desorption		
Material	w_{max} (kg H / kg M)	ΔH (MJ / kg M)	C_A (1/s)	E_A (kJ / mol H)	ΔH (MJ / kg M)	C_A (1/s)	E_A (kJ / mol H)
$MmNi_{4.5}Cr_{0.5}$	0.0121	11.67	620	30.87	12.65	90	28.25
$LaNi_5$	0.0151	15.46	50	20.00	15.95	9.57	16.42

The reaction rate, r, which appears in both the energy and mass balance, is the rate of change of the weight fraction of hydrogen stored in the hydride. It is a function of the hydrogen pressure, P_H, and weight fraction, w, of the hydride, as well as the equilibrium pressure, P_{eq}, of the hydride, which is itself a function of the temperature, T_r, and weight fraction, w, of the hydride. The reaction rate, as described by Voskuilen *et al* [9], is calculated using the equation

$$r = \frac{dw}{dt} = \begin{cases} C_A e^{-\frac{E_A}{RT_r}} ln\left(\frac{P_H}{P_{eq}}\right) w, & P_H < P_{eq,des} \\ 0, & P_{eq,des} \le P_H \le P_{eq,abs} \\ C_A e^{-\frac{E_A}{RT_r}} ln\left(\frac{P_H}{P_{eq}}\right)(w_{max} - w), & P_H > P_{eq,abs} \end{cases} \quad (15)$$

where C_A and E_A are constants that are properties of the hydride material (see Table 1).

The equation used for $\dot{m}_{H,in}$, as well as those for ε and P_{eq}, can be found in the more detailed description of this model in Krane *et al.* [44].

The rate of work $\dot{W}$ done by the compressor on the hydrogen is calculated based on an assumed compressor isentropic efficiency of η_s = 0.8, and the specific enthalpy, h, at the compressor inlet and outlet, using Equations 16–19.

$$\eta = \frac{h_{comp\ out,s} - h_{comp\ in}}{h_{comp\ out} - h_{comp\ in}} = \frac{c_P\left(T_{comp\ out,s} - T_{comp\ in}\right)}{c_P\left(T_{comp\ out} - T_{comp\ in}\right)} \quad (16)$$

$$h_{comp\ out,s} = c_P T_{comp\ in}\left(\frac{P_{comp\ out}}{P_{comp\ in}}\right)^{\frac{R}{c_P}} \quad (17)$$

$$h_{comp\ out} = h_{comp\ in} + \frac{\left(h_{comp\ out,s} - h_{comp\ in}\right)}{\eta_s} \quad (18)$$

$$\dot{W} = \dot{m}_{H,in}\left(h_{comp\ out} - h_{comp\ in}\right) \quad (19)$$

At each time step in the secondary loops model, the load-shifting control logic described in Section 3.2.4 determines the desired heat transfer rate in each of the hydride reactors. Then, a model predictive controller (MPC) sets the flow rates of water glycol diverted to the reactors and the pressure difference generated by the compressor on the hydrogen line needed to match these heat transfer rates. The controller uses a linearized form of the governing equations described by equations 13–15 to predict future states of the model and solve for the optimal values of the control input variables. Within each time step of the secondary loops model, the transient model of the hydride reactors is simulated, with the controller updating its input values every 10 s. The MPC algorithm is described in detail in Krane *et al.* [44].

3.2.4. Load-Shifting control logic

Here, we develop a heuristic load-limiting storage control strategy to determine the distribution of load between the heat pump and the reactors. Perfect knowledge of future building loads for each day is assumed for the purpose of assessing system performance. For the load-limiting control strategy, the system attempts to discharge the entire storage system during the on-peak period and fully charges it in the off-peak period. This strategy is similar to that described by Tam *et al.* [45], but differs from it in charge mode by not running the heat pump at full capacity until the system is fully charged. Instead, the system uses a constant heat pump load for charging that is calculated as described in the next paragraph. The heat pump is not run at full capacity when charging in order to reduce the change in reactor temperature when charging begins. This is done in order to prevent the reactor temperature

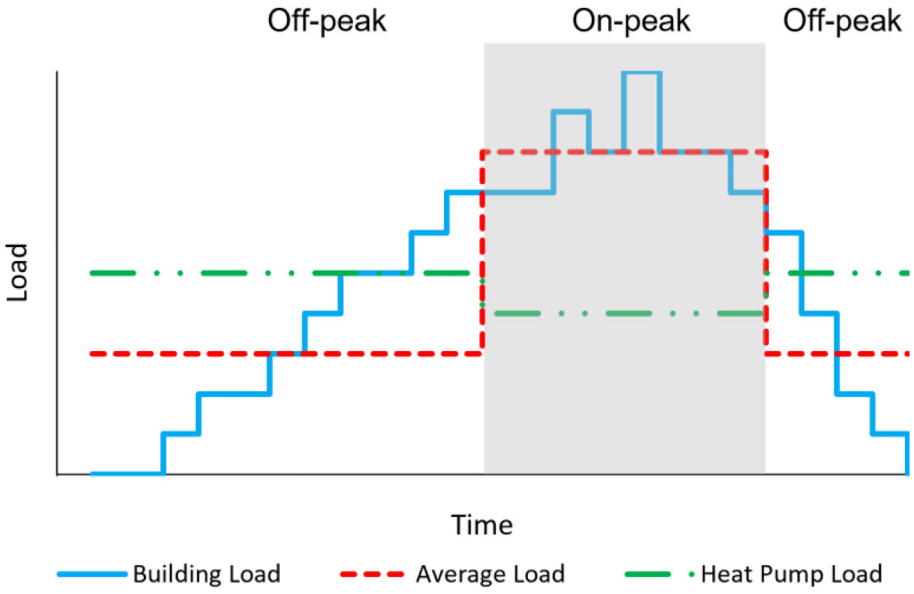

Fig. 6. Diagram showing how heat pump loads for charging and discharging are calculated. The charging load is calculated by increasing the average off-peak heat pump load by the load needed to fully charge the storage system over the full period. The discharging load is calculated by reducing the average on-peak heat pump load by the load provided by the storage system if fully discharged.

from becoming too close to the water-glycol temperature, thereby increasing the required pump work.

Fig. 6 illustrates the calculation of the heat pump loads for one day. The charging load is calculated by increasing the average off-peak heat pump load by the load needed to fully charge the storage system over the full period. The discharging load is calculated by reducing the average on-peak heat pump load by the load provided by the storage system if fully discharged. Thus, at the beginning of each cycle (defined as a 24-hour period), the total building loads for the off-peak and on-peak periods, Q_{charge} and $Q_{discharge}$ (respectively), are calculated using the following equations.

$$\dot{Q}_{charge} = \frac{\sum_{off} \dot{Q}_{load,house} + E_{stor,hyd}}{\Delta t_{off}} \quad (20)$$

$$\dot{Q}_{discharge} = \frac{\sum_{on} \dot{Q}_{load,house} - E_{stor,hyd}}{\Delta t_{on}} \quad (21)$$

In these equations, $E_{stor,hyd}$ is the difference in stored energy between a fully charged and a fully discharged storage system. For the purposes of this control logic, "fully charged" and "fully discharged" are defined as 90% and 10% of the maximum weight fraction that can be stored in the metal hydride, respectively. These values are used due to the higher compressor costs required as the weight fraction approaches its maximum or minimum value.

The method just described is used for the case where there is one on-peak period during each day (except for weekends). However, in some existing rate structures, there are two on-peak periods in a day during the winter (one in the morning and one in the evening). Since it is not feasible to fully charge the system in between these periods due to the high loads that occur during the day, the system still treats a full day as a cycle when operating under these rates. Thus, for cooling mode, the system is fully charged during the off-peak hours at night, and fully discharged over the course of the two on-peak periods during the day, while running conventionally in between these periods (for heating mode, it is charged in the afternoon and runs conventionally during the night, since heating loads are lower during the day).

Once the charging and discharging loads for the day have been determined, the model determines the operating mode of the system at each time step using the control logic shown in Fig. 7. During on-peak hours, the heat pump provides the load calculated for discharging, with the storage system discharged to make up the difference between this and the building load. However, if the building load is less than the heat pump load for discharging, the system will not be discharged; instead, the heat pump will meet the building load without any heat transfer to and from the storage system (conventional operation). During off-peak hours, the storage system is discharged in cooling mode if the building load exceeds the capacity of the heat pump. In this case, the heat pump load is equal to its capacity and the storage system makes up the difference. If this condition occurs immediately before the on-peak period, the on-peak heat pump load is adjusted to make up for the difference between available and full storage capacity.

For heating mode (even in conventional systems), electric heating is used to provide heating when the building heating load is greater than what can be provided by the heat pump. In this control strategy, if the calculated heat pump load for charging or discharging exceeds the capacity of the heat pump, the heat pump load is set to the capacity of the heat pump and the difference between these values is provided by electric heating throughout the time period. Auxiliary heating is considered to be a part of the indoor heat exchanger and thus to have no effect on temperatures in the indoor loop.

During off-peak hours, the system is charged with the heat pump providing the calculated load for charging, with any load in excess of the building load being used to charge the storage system. However, if the storage system is already fully charged or if the building load is greater than the heat pump load for charging, the system runs in conventional operation instead. While the heat pump load for charging is calculated so the system will charge over the full off-peak period, in practice, the system will often be fully charged before the end of the off-peak period. This happens primarily for two reasons. First, the heat pump load is calculated assuming that the system runs at this load throughout the off-peak period. However, to do this, the system would have to discharge if there is a building load greater than the heat pump load for charging, but the system will run instead conventionally in that case. Since the system does not discharge at these times, it does not have to be charged to make up for any such discharging. Because of this, the system will charge in less than the full off-peak period. The second reason is that if the system enters a charging period partially or fully charged, due to either a discharge period where

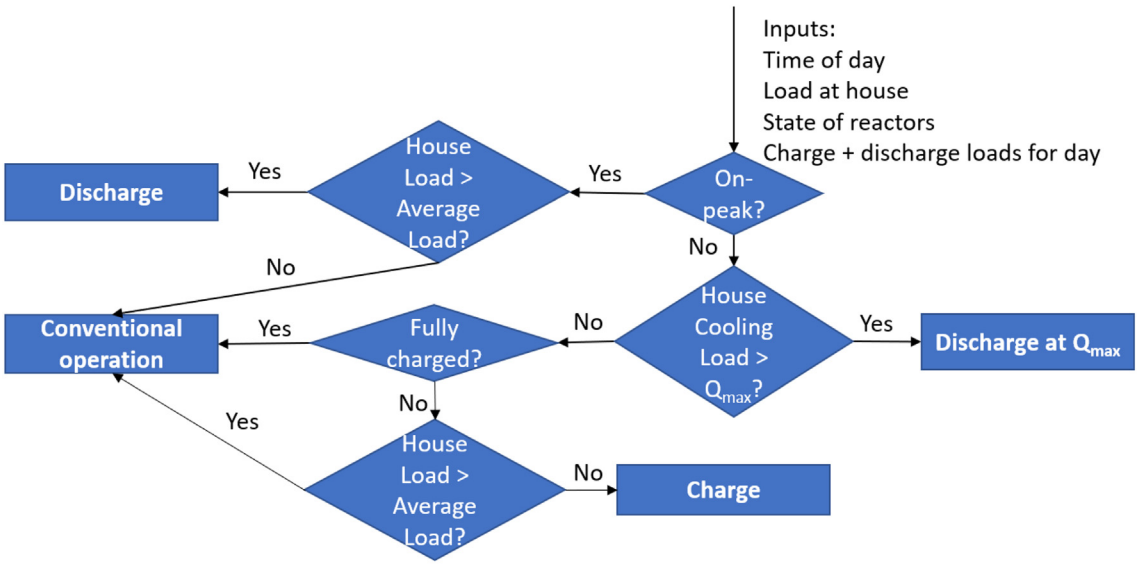

Fig. 7. Flowchart showing the control logic for whether the energy storage system is charged, discharged, or not used at each time step.

the full storage capacity was not required or due to previous charging on the weekend (which has no on-peak periods), it will charge in less than the full off-peak period because the heat pump load for charging is calculated assuming the system needs to be fully charged.

4. Results and discussion

The system model described in Section 1 is evaluated first in Section 4.1 for a single week each in summer and winter to demonstrate how the system can achieve cost savings through load shifting. The initial cost of the system is estimated as described in Section 4.2 so that the payback period can be determined from annual cost savings. Annual cost savings and payback periods for a range of utility rate structures are calculated in Section 4.3, and these results are discussed in Section 4.3.4.

4.1. Short-term system performance

To demonstrate the behavior of the proposed system architecture, we first evaluate the performance for a week in the summer and a week in the winter for a hypothetical house in Elizabeth City, NC. We selected a city in the American South as the object of this study because this is the only region in the United States where electric heating, such as is used in our system, is more commonly used than gas heating [46]. Data from Typical Meteorological Year 3 [47] for January 1–7 and June 1–7 was used for the temperature and solar irradiation, while data from the Office of Energy Efficiency & Renewable Energy on residential hourly electricity loads was used to estimate the hourly non-HVAC electricity loads [42]. The TOU utility rate structure for this location was taken from the Utility Rate Database maintained by the National Renewable Energy Laboratory [48], and is summarized in Table 2.

For this study, the conventional system to which the system with energy storage is compared uses a fixed-speed heat pump with a seasonal energy efficiency ratio (SEER) of 17.5 and a rated maximum cooling capacity of 3 RT (10.55 kW). This heat pump is sized to meet the maximum cooling load for the year in this location. For the energy storage system, the heat pump is downsized to a rated capacity of 2.5 RT (8.79 kW), since this system can use energy storage to reduce the peak cooling load required for the heat pump. The energy storage system is sized to store enough energy to meet the difference between the building load and heat pump capacity on the day with the highest cooling loads whenever the load is above the capacity of the heat pump. The reactors are sized so that the low-temperature reactor can provide the load in cooling mode and the high-temperature reactor matches the storage capacity of the low-temperature reactor. Thus, this system requires one reactor with 470 kg $MmNi_{4.5}Cr_{0.5}$ and the other with 412 kg $LaNi_5$.

Results for running the system for the representative summer and winter weeks are shown in Fig. 8. Each of these weeks begins at 1 am on Sunday. Considering the summer results shown in Fig. 8a, the energy storage system is discharged during the weekday on-peak periods, except on Tuesday when there is no on-peak cooling load, and also once on a Sunday afternoon, when the load on the house exceeds the capacity of the heat pump. The storage system is charged during off-peak hours, and primarily at night, when there is no home cooling load. Considering the results for winter shown in Fig. 8c, the heat pump load varies primarily due to changes in heating capacity with changing ambient temperature. This is because most of the time, except for Tuesday, the house load exceeds the heat pump capacity and electric heating is used to make up the difference. The energy storage system does reduce the heat pump load by discharging on Monday and Wednesday. It is not needed due to lack of a load on Tuesday. The main effect of the TES system when discharging is to reduce the use of electric heating: on Monday and Wednesday, electric heating is eliminated and on Thursday and Friday, electric heating usage is reduced to less than a third of the rate immediately before the on-peak period starts. The energy storage system therefore primarily reduces the electric heating costs by moving a portion of this load from on-peak to off-peak hours. Since the heating loads in winter are larger than the cooling loads in summer (and the storage system is not sized for full storage even in the summer), some electric heating is still required (in addition to the heat pump) even during some of the on-peak periods. For both winter and summer, looking at the state-of charge for each week (see Fig. 8b and Fig. 8d), the system charges in significantly less time than the off-peak duration and in between charging and discharging, the conventional heat pump (and electric heating in winter) meets the load on the house.

The costs of running this system for the summer and winter weeks, compared to the costs of running a conventional system where the heat pump meets the entire cooling load, are given in Appendix C. These results show that metal hydride energy storage reduces the operating costs of the heat pump and auxiliary heating, while adding increased operating costs for running the compressor. These costs for the compressor are significant enough to result in higher overall operating costs for the summer week. However, in the winter week, the increased cost savings from reducing the use of less-efficient auxiliary heating during the on-peak period outweigh the costs of running the compressor. Cost savings in the winter are larger if the heat pump is not downsized, since downsizing the heat pump results in a greater use of auxiliary heating.

Table 2
Residential TOU rate structure for Elizabeth City, NC.

Season	On-Peak Hours	On-Peak Rate	Off-Peak Rate
Winter	6–10 AM, Mon-Fri	27.6 ¢/kWh	5.52 ¢/kWh
Summer	2–7 PM, Mon-Fri	27.6 ¢/kWh	5.52 ¢/kWh

4.2. System cost estimates

The installed cost of the conventional system is the sum of the costs of the heat pump and the auxiliary electric heating system. For the energy storage system, the initial cost also includes the costs of the secondary loops with pumps and internal and external air-handling units, metal hydride reactors, and the compressor for pumping hydrogen. For the heat pump, the cost is estimated as a function of the rated capacity and SEER, based on a correlation developed by the Energy Efficiency and Renewable Energy Office [49]:

$$y_{hp} = 1.91 * 10^3 - 41.4SEER_{rated} + 7.48SEER_{rated}{}^2 + 589Q_{rated} - 16.4Q_{rated}{}^2. \quad (22)$$

An estimated cost of $10/kW capacity was determined for the auxiliary electric heating. This cost was determined by examining the prices and maximum capacities of commercially-available units and identifying a correlation that resulted in similar prices to those of these existing units across the range of capacities examined here.

The most expensive component in the energy storage system is the metal hydride reactors. The reactor cost is determined by estimating the material costs for the hydrides, since this is much higher than the installation or material costs for the heat exchanger. Based on private correspondence with a supplier, a price of $20/kg was estimated for $LaNi_5$, based on existing products, but similar information was not available for $MmNi_{4.5}Cr_{0.5}$, which is

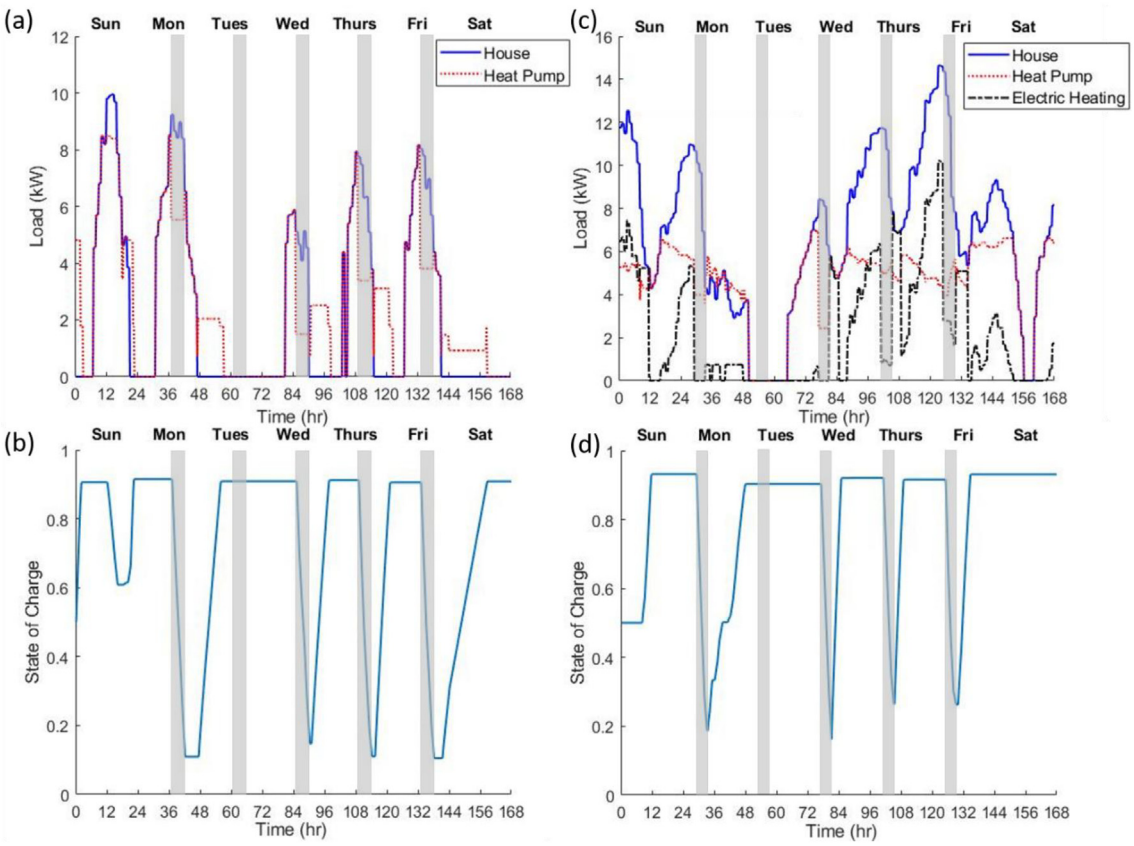

Fig. 8. Results for sample weeks in summer and winter, starting at 1 am on Sunday. On-peak periods are shaded in gray. (a) Cooling load required by the house and produced by the heat pump for a week in summer. (b) State of charge of the hydride reactor system over time for the summer week. (c) Required heating load at the house, heat pump load, and electric heating over time for a week in winter. (d) State of charge of the hydride reactor system over time for the winter week.

not currently in use in large quantities. Comparing raw material prices for lanthanum and mischmetal [50] indicated that this material would likely be comparably priced to $LaNi_5$ if it were as commonly used. Therefore, a price of $24/kg was used for this material, as an approximation of the potential bulk price should the material become more commonly used. Both of these costs are reduced by 25% to account for the gains from recycling them at the end of their life cycle, so the actual values used are $15/kg for $LaNi_5$, and $18/kg for $MmNi_{4.5}Cr_{0.5}$.

The total cost of piping for an indoor secondary loop, including pump and air-handling unit, was estimated by Tam *et al.* to be $1,301 [20]. Based on a cost breakdown for a secondary-loop system, the cost of the outdoor secondary loop, where the indoor air-handling system is replaced with an outdoor heat exchanger, was estimated to be $1,050. Since hydrogen compressors are usually used at much larger pressure ratios than the 10-bar limit imposed in this case, the cost of the compressor was estimated by comparing prices for air compressors with the appropriate operating pressures, resulting in an estimated cost of $200.

Using these prices, and the sizing decisions discussed in Section 4.1, we can compare the initial cost of 3 systems: 1) conventional system without energy storage; 2) system with energy storage and a downsized heat pump; and 3) system with energy storage and without a downsized heat pump. The initial costs of these systems are shown in Table 3. In the following section, these systems will be compared to determine the annual change in operating costs and resulting economic payback period for each of the systems that include energy storage.

4.3. Annual cost savings and payback period

In this section, annual costs savings and the resulting payback period are determined first for existing utility rates in Section 4.3.1, then for potential alternative rates with the same on-peak period in Section 4.3.2, and finally for alterative rates with varying on-peak periods in Section 4.3.3.

4.3.1. Cost savings for existing utility rates

To determine the economic viability of the proposed systems, the system model for each was simulated for a calendar year for each of the three systems previously discussed using the weather data, utility rates, and hourly electricity loads for other systems applied to the house described in Section 3.1 for Elizabeth City, NC. The resulting annual operating costs, broken down by month

Table 3
Initial costs, by component, of the conventional system and the system with energy storage (both with and without downsizing the heat pump).

System	Initial Cost Heat Pump	Electric Heating	Hydrogen Compressor	Secondary Loops	Metal Hydrides	Total
Conventional	$5,096	$100	–	–	–	$5196
Storage w/ smaller heat pump	$4,864	$110	$200	$2,351	$14,640	$22,147
Storage w/out smaller heat pump	$5,096	$100	$200	$2,351	$14,640	$22,387

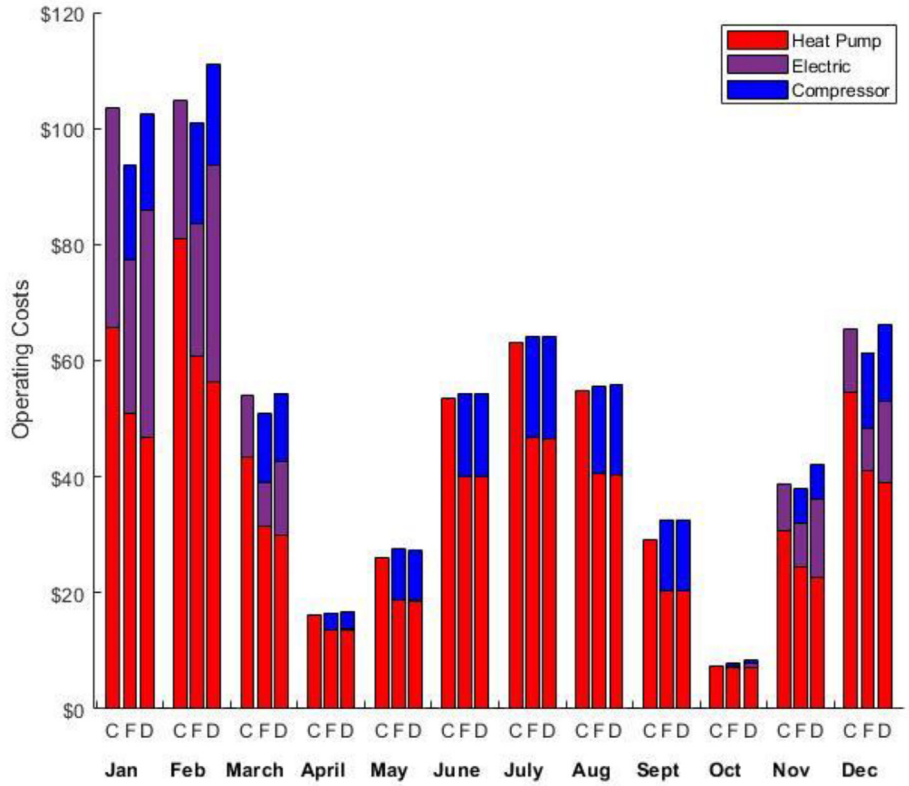

Fig. 9. Comparison of HVAC system operating costs, by month, between the systems with energy storage to the conventional (C) system. The energy storage cases are shown with the full-size heat pump (F) and with a downsized heat pump (D).

and by component, for the three systems are shown in Fig. 9. These costs show that downsizing the heat pump is not the right choice for this location, since it results in an increase in the total operating cost, with the hydrogen compressor and the increased electric heating outweighing the reduction in the heat pump costs. Even without downsizing, however, the system only achieves small cost savings, reducing the annual cost savings by only $13. While the system with storage consistently has lower heat pump costs and lower electric heating costs if not downsized, which system has lower operating costs overall varies from month to month, with the energy storage system primarily reducing costs in the winter months. These cost savings in the winter are due to the use of electric heating, which increases the on-peak operating costs and thus provides a stronger incentive for the use of energy storage. Without this, as in the summer, the increased work from the compressor outweighs the reduced costs of operating the heat pump.

4.3.2. Cost savings for potential alternate utility rates

For this system to achieve large cost savings, the utility rates would have to be more favorable to energy storage, by having higher on-peak and lower off-peak rates. To evaluate the sensitivity of the payback period to the TOU rate structure, the operating costs for the year are calculated for a series of rate structures. These rate structures, given in Table 4, are designed to result in the same annual operating cost for the system without energy storage, and differ in the ratio of the on-peak to off-peak rates. The rate structure in which this ratio equals 5 is the existing rate structure used for the previous results. All of these rates use the same on-peak periods, as defined in Table 2. The higher the ratio of on-peak to off-peak rates, the more the rate structure incentivizes shifting the load away from the on-peak period. The resulting change in operating cost, compared to the conventional system, and the payback period for the energy storage system with the different TOU rates is shown in Fig. 10. The payback period is not shown for rates that did not result in cost savings or that resulted in cost savings low enough that the payback period exceeded 600 years.

As shown in Fig. 10, any rates with a lower ratio than the existing rate structure do not result in any cost savings for this system. For cases with a higher ratio, the cost savings increase, reaching nearly $150 at a ratio of 20. The payback period becomes shorter as these cost savings increase but, as seen in Fig. 10, are still too large, exceeding 100 years for all of the rate structures considered. Even if electricity were free during off-peak periods and the on-peak rate were $0.5772/kWh, the resulting payback period for this system would be 75 years.

In addition to these results, cost savings were also calculated for rate structures with a constant electricity rate and an on-peak demand charge. These results are described in Appendix D. The system achieves significantly larger cost savings for these rate structures: for the case where the constant rate is the same as the existing off-peak rate, it achieves annual cost savings of $101.65. However, it does not achieve a short payback period; for the case where all costs are due to the on-peak demand charge, the payback period is still 37 years. These results show that the cost savings the system achieves are strongly dependent on the utility rate structure in place. For rates that are more favorable to energy storage, it can achieve substantial cost savings; however, these cost savings do not result in a favorable payback period because of the high initial cost of the system.

4.3.3. Cost savings for potential alternate on-peak periods

Electricity rate structures also vary in the time at which the on-peak period occurs. To evaluate the sensitivity of the payback per-

Table 4
Rate structures used to examine how the cost savings from energy storage change with changes in how strongly the TOU rates incentivize load shifting. All of these rate structures result in the same annual operating cost for the conventional system.

Ratio of On-peak to Off-peak Rates	On-peak Rate	Off-peak Rate	Ratio of On-peak to Off-peak Rates	On-peak Rate	Off-peak Rate
1	$0.0894	$0.0894	8	$0.3431	$0.0429
2	$0.1548	$0.0774	10	$0.3734	$0.0373
3	$0.2048	$0.0683	12	$0.3968	$0.0331
4	$0.2442	$0.0610	15	$0.4232	$0.0282
5*	$0.2760	$0.0552	18	$0.4429	$0.0246
6	$0.3023	$0.0504	20	$0.4535	$0.0227

*Existing rate structure used for previous results.

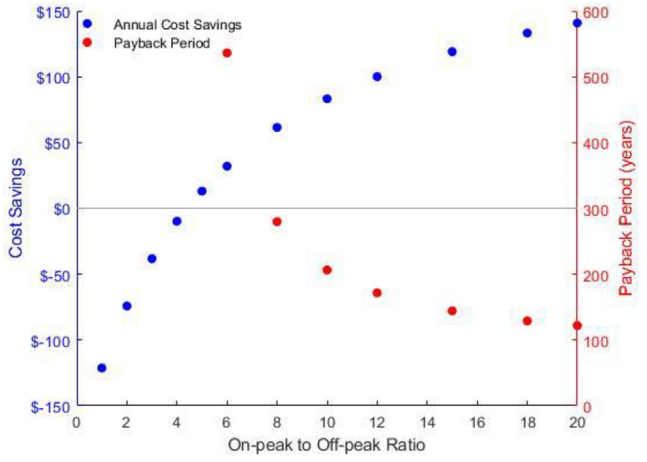

Fig. 10. Annual cost savings and payback period from using energy storage, as compared to the conventional system, for the rate structures given in Table 4. Payback period is not shown for rates that did not result in cost savings, or resulted in cost savings low enough that the payback period exceeded 600 years.

iod on this feature of the rate structure, the system was analyzed for a range of cases with different on-peak times, and different rates considered for each of these cases. The on-peak periods considered are given in Table 5. Case 4 corresponds to the on-peak period for the existing utility rates used to generate results in Section 4.3.2. These cases were designed to consider the effect of having the winter on-peak period at different times of day (afternoon, morning, evening, morning and evening), and having the summer on-peak period be a longer or shorter period and of it being later in the afternoon.

For each of these cases, cost savings were calculated for different rate structures that were determined using the same method as in Section 4.3.2 and Appendix D. For each case, the same number of rate structures, both with and without demand charges, were used as were described in section 4.3.2. For each case, structures with TOU rates were determined by varying the ratio of the on-peak rates to the off-peak rates while holding the annual operating cost for a conventional system constant. The rate structures with an on-peak demand charge for each case have the same operating costs for the conventional system and constant electricity rates equal to the off-peak rates for the TOU rate structures studied. For each case, the rate structures were defined so that the rates for an on-peak to off-peak ratio of 5 were the same as existing rates. Note that this means the conventional system operating costs, while the same for all rates studied for a particular case, are not the same for different cases due to the different lengths of the on-peak periods.

Table 5
Alternate on-peak periods for which cost savings with different rate structures were analyzed.

	Summer On-peak Period	Winter On-peak Period
Case 1	12–8 PM	12–8 PM
Case 2	2–7 PM	2–7 PM
Case 3	12–8 PM	6–10 AM, 6–9 PM
Case 4	2–7 PM	6–10 AM
Case 5	3–9 PM	6–9 PM

The operating cost savings for different TOU rate structures for each case are shown in Fig. 11. The cost savings from rate structures with on-peak demand charges are shown in Fig. 12 where cost savings are plotted against the percentage of the conventional system operating costs that are due to the on-peak demand charge. In other words, the points corresponding to 0% represent constant rates with no demand charge and points corresponding to 100% represent rates in which all of the cost is due to an on-peak demand charge. This provides a metric that is meaningful across the different rate structures included in Fig. 12.

Across all the cases studied, we can see that the largest cost savings come from rate structures with on-peak demand charges. Cases 3 and 4 have the largest cost savings for both TOU rates and rates with an on-peak demand charge, with the largest cost savings coming from rates for Case 4 with an on-peak demand charge. These cases both have afternoon on-peak periods in the summer, and morning on-peak periods in the winter (with Case 3 also having a winter evening on-peak period). Cost savings were greatest for these cases because the winter on-peak periods in these cases required the greatest use of auxiliary electric heating for a conventional system. With energy storage, most of this on-peak auxiliary heating (>80% for Case 3, >90% for Case 4) did not have to be used since the load was met by the storage system instead. Since reducing the use of auxiliary electric heating provides a higher potential for cost savings than reducing the use of the heat pump, these cases have larger cost savings than those where there is less electric heating during the on-peak periods.

Since Case 4 has the same on-peak period as existing rates, these rates are the same ones discussed in more detail in Appendix D, which did not achieve any payback periods less than 37 years. Since none of the other on-peak periods considered result in higher cost savings than these rates, none of them result in better payback periods. The large cost savings for some of these cases (>$350 for the case where all the cost is due to an on-peak demand charge, >$250 for several rates with high on-peak demand charges and very low electricity rates) show the sensitivity of these results to the rate structures used. That even these large cost savings still result in a high payback period is due to the high initial cost of the system.

4.3.4. Discussion

The system proposed in this paper achieves the goal of providing year-round energy storage with a single system—both in heating and cooling modes—and enables cost savings on an annual basis. However, due to the high initial system cost and the reduced operating cost savings from compressing hydrogen, the system has

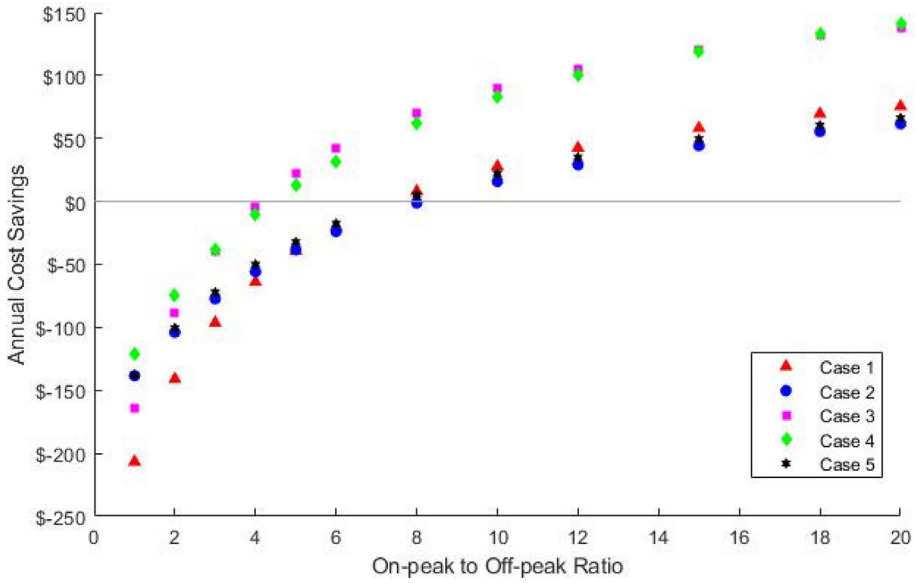

Fig. 11. Annual operating cost savings from using energy storage for different TOU rate structures.

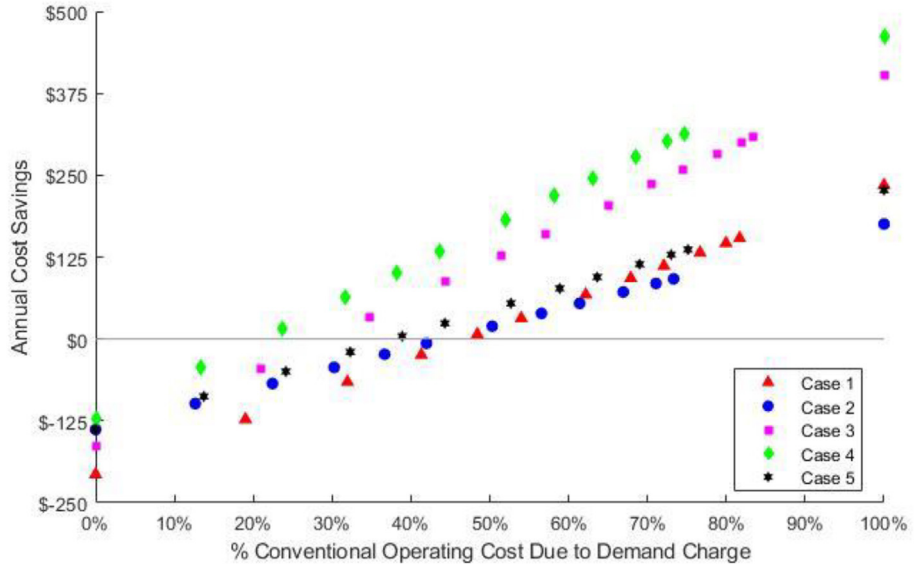

Fig. 12. Annual operating cost savings from using energy storage for different rate structures with on-peak demand charges.

a high payback period across a range of utility rate structures and so is currently not cost-effective for commercialization.

The high initial cost of the metal hydrides is a major factor in the high payback periods of the system, since 85.2% of the increase in initial cost for the system with energy storage is due to the cost of the hydrides. For the system to have a payback period of less than 10 years at existing rates, the initial cost of all components would have to decrease by 94%. This value is reduced for rates more favorable to energy storage; however, even at the most favorable rates (where all operating costs are due to a high on-peak demand charge), a reduction in component cost by 73% would be required to achieve a 10-year payback period. Thus, while other things can be done to improve the cost-effectiveness of this system, a large reduction in the initial cost of the system, and particularly the cost of the metal hydrides, would be necessary for it to achieve a viable payback period. If the safety concerns from high-pressure storage could be managed, the initial cost of the system could be substantially reduced by replacing one of the hydride reactors with a hydrogen storage tank, although this would likely have the downside of increasing the cost of hydrogen compression as well.

The loss of operating cost savings from running the compressor is the other major contributor to the high payback period of the system. A storage system that was able to do the same load-shifting as the metal hydrides without the compressor operating costs would achieve much greater cost savings; for instance, at existing utility rates, the metal hydrides reduce heat pump and electric heating costs by $149, but $136 of this is lost running the compressor. Therefore, compressor costs would need to be substantially reduced for metal hydrides to compete with other forms of TES. Compressor costs would not be an issue if hydrogen flow were purely temperature-driven; however, this would require that the system operate at a wider range of temperatures and pressures, since the materials used in this paper were selected to minimize

the required compressor work while operating within a narrow range of temperatures and pressures. Thus, reducing compressor work would require higher-pressure hydrogen storage in the hydride reactors, as well as a higher-temperature heat source to create a sufficient temperature difference to drive the reaction. If the system cannot be made purely temperature-driven, modifications to the target heat rates and controller to reduce compression costs might also be examined. Moreover, as mentioned in Section 1, optimization of the metal hydride operating temperatures was not considered in this paper. Similarly, heuristic control logic was used for charging and discharging the system rather than an optimal controller. Optimization of the operating temperatures and load-shifting control logic would improve the cost savings that this system can achieve.

These results also show that there is a high potential for cost savings from energy storage coupled with residential heating in buildings that use a heat pump supplemented by auxiliary electric heating. As seen in Fig. 9, the metal hydride energy storage system achieves cost reductions of up to $10/month in months with heating loads large enough to require electric heating (even at rates where it fails to achieve any cost savings in months where electric heating is not used). This is due to the higher marginal cost savings from reducing the use of electric heating during on-peak periods than those from reducing the use of a heat pump. Because of this, 57.8% of the reduction in heat pump and electric heating costs (neglecting compressor costs) achieved by the system at existing rates occurs in the months of October-March. The results indicate that an energy storage system used with a residential heating system could achieve larger cost savings than an energy storage system with a cooling system for a location where heat pumps with auxiliary electric heating are used, but where there are significant heating loads in the winter that do require the use of auxiliary heating (such as the location studied here).

5. Conclusions

In this paper, we have proposed and evaluated a metal hydride energy storage system used with a residential HVAC system for year-round energy storage to shift load from on-peak to off-peak hours with TOU rates. The architecture consists of two metal hydride tanks integrated with a heat pump. For the evaluation, a model of this system was developed that incorporates the heating or cooling load on the house, the performance of the heat pump, and the energy balances for the secondary loops and the metal hydride reactors, as well as a control strategy for optimizing use of the storage system. This model illustrates that year-round energy storage for a building heated and cooled by a vapor-compression heat pump is possible with metal hydrides. Calculations for example weeks in the summer and winter show that this system effectively shifts the heat pump load in the summer and the electric heating load in the winter away from on-peak hours to off-peak hours. This load-shifting only reduces annual operating costs by $13 at existing utility rates, primarily due to the operating costs of compressing hydrogen. Even ideal TOU rates designed to maximize cost savings result in unacceptably large payback periods for the system: the payback period remains over 100 years for rates in which the on-peak rate is 20 times the off-peak rate, and is 37 years for the case in which all operating costs are due to an on-peak demand charge. The long payback periods are due to the high initial cost of the metal hydrides and the reduced operating cost savings from hydrogen compression. The performance of metal hydride energy storage could potentially be improved through the use of compressed hydrogen storage with one hydride reactor, or through finding better-matched metal hydride pairs that could reduce or eliminate the need for the compressor. Furthermore, the fact that this system achieved greater cost savings in heating mode than in cooling indicates that there is a potential for large cost savings from year-round energy storage in residential buildings using a heat pump for auxiliary electric heating. However, achieving these cost savings would require an energy storage system without the high operating costs for hydrogen compression seen in this system.

Declaration of Competing Interest

The authors declare that they have no known competing financial interests or personal relationships that could have appeared to influence the work reported in this paper.

Acknowledgements

Funding for this research was provided by the Center for High-Performance Buildings at Purdue University.

Appendix A. Supplementary data

Supplementary data to this article can be found online at https://doi.org/10.1016/j.enbuild.2021.111700.

References

[1] S.M. Hasnain, Review on sustainable thermal energy storage technologies, Part II: Cool thermal storage, Energy Convers. Manag. 39 (11) (1998) 1139–1153.
[2] I. Dincer, On thermal energy storage systems and applications in buildings, Energy Build. 34 (4) (2002) 377–388.
[3] G. Krese, R. Koželj, V. Butala, U. Stritih, Thermochemical seasonal solar energy storage for heating and cooling of buildings, Energy Build. 164 (2018) 239–253.
[4] K.H. Lee, M.C. Joo, N.C. Baek, Experimental evaluation of simple thermal storage control strategies in low-energy solar houses to reduce electricity consumption during grid on-peak periods, Energies 8 (9) (2015) 9344–9364.
[5] S.M. Hasnain, Review on sustainable thermal energy storage technologies, Part I: Heat storage materials and techniques, Energy Convers. Manag. 39 (11) (1998) 1139–1153.
[6] Y. Hamada, J. Fukai, Latent heat thermal energy storage tanks for space heating of buildings: comparison between calculations and experiments, Energy Convers. Manag. 46 (20) (2005) 3221–3235.
[7] G.G.D. Han, H. Li, J.C. Grossman, Optically-controlled long-term storage and release of thermal energy in phase-change materials, Nat. Commun. 8 (1) (2017), https://doi.org/10.1038/s41467-017-01608-y.
[8] S. Luo, W. Luo, J.D. Clewley, T.B. Flanagan, L.A. Wade, Thermodynamic studies of the LaNi5-XSnx-H system from x = 0 to 0.5, J. Alloys Compd. 231 (1-2) (1995) 467–472.
[9] T.G. Voskuilen, E.L. Waters, T.L. Pourpoint, A comprehensive approach for alloy selection in metal hydride thermal systems, Int. J. Hydrogen Energy 39 (25) (2014) 13240–13254.
[10] U.S. DOE, 2020, Energy Storage Grand Challenge: Energy Storage Market Report.
[11] R.A. Potter, D.J. King, D.P. Weitzel, D.D. Boettner, Study of operational experience with thermal storage systems, ASHRAE Trans. (1995) 549–557.
[12] S. Sanaye, A. Shirazi, Thermo-economic optimization of an ice thermal energy storage system for air-conditioning applications, Energy Build. 60 (2013) 100–109.
[13] F. Kung, M. Deru, E. Bonnema, 2013, "Evaluation Framework and Analyses for Thermal Energy Storage Integrated with Packaged Air Conditioning," Natl. Renew. Energy Lab., (October).
[14] N. Nassif, R.C. Tesiero, H. Singh, Impact of ice thermal storage on cooling energy cost for commercial HVAC systems, ASHRAE Trans. 119 (2013).
[15] K. Drees, J. Braun, Development and evaluation of a rule-based control strategy for ice storage systems, HVAC&R Res. 2 (4) (1996) 312–334.
[16] G.P. Henze, An overview of optimal control for central cooling plants with ice thermal energy storage, J. Sol. Energy Eng. 125 (3) (2003) 302–309.
[17] S. Boonnasa, P. Namprakai, The chilled water storage analysis for a university building cooling system, Appl. Therm. Eng. 30 (11-12) (2010) 1396–1408.
[18] S. Rosiek, F.J. Batlles Garrido, Performance evaluation of solar-assisted air-conditioning system with chilled water storage (CIESOL building), Energy Convers. Manage. 55 (2012) 81–92.
[19] S. Al-Hallaj, S. Khateeb, A. Aljehani, M. Pintar, 2018, "Thermal Energy Storage for Smart Grid Applications," AIP Conf. Proc., 1924.
[20] A. Tam, J.E. Braun, D. Ziviani, N. Jain, 2018, An overall assessment of ice storage systems for residential buildings, 5th Int. High Perform. Build. Conf. Purdue, (July).

[21] P. Moreno, C. Solé, A. Castell, L.F. Cabeza, The use of phase change materials in domestic heat pump and air-conditioning systems for short term storage: a review, Renew. Sustain. Energy Rev. 39 (2014) 1–13.
[22] C. Finck, R. Li, R. Kramer, W. Zeiler, Quantifying demand flexibility of power-to-heat and thermal energy storage in the control of building heating systems, Appl. Energy 209 (2018) 409–425.
[23] H. Caliskan, I. Dincer, A. Hepbasli, Energy and exergy analyses of combined thermochemical and sensible thermal energy storage systems for building heating applications, Energy Build. 48 (2012) 103–111.
[24] F. Agyenim, N. Hewitt, The development of a finned phase change material (PCM) storage system to take advantage of off-peak electricity tariff for improvement in cost of heat pump operation, Energy Build. 42 (9) (2010) 1552–1560.
[25] Z. Yin, W. Zhiyuan, W. Xin, Z. Yinping, Optimal phase change temperature for BCHP system with PCM-TES based on energy storage effectiveness, Procedia Eng. 205 (2017) 533–539.
[26] Y. Zhang, X. Wang, Y. Zhang, S. Zhuo, A simplified model to study the location impact of latent thermal energy storage in building cooling heating and power system, Energy 114 (2016) 885–894.
[27] A. Hauer, 2007, ‘‘Adsorption Systems for TES- Design and Demonstration Projects,’’ Thermal Energy Storage for Sustainable Energy Consumption, Halime O. Paksoy, ed., Springer, Dordrecht, pp. 409–427.
[28] B. Mette, H. Kerskes, H. Drück, Concepts of long-term thermochemical energy storage for solar thermal applications – selected examples, Energy Procedia 30 (2012) 321–330.
[29] F. Desai, J. Sunku Prasad, P. Muthukumar, M.M. Rahman, Thermochemical energy storage system for cooling and process heating applications: a review, Energy Convers. Manag. 229 (2021) 113617, https://doi.org/10.1016/j.enconman.2020.113617.
[30] M. Tange, T. Maeda, A. Nakano, H. Ito, Y. Kawakami, M. Masuda, T. Takahashi, Experimental study of hydrogen storage with reaction heat recovery using metal hydride in a totalized hydrogen energy utilization system, Int. J. Hydrogen Energy 36 (18) (2011) 11767–11776.
[31] A. Khayrullina, D. Blinov, V. Borzenko, Air heated metal hydride energy storage system design and experiments for microgrid applications, Int. J. Hydrogen Energy (2018) 1–9.
[32] D. Magnetto, S. Mola, A metal hydride mobile air conditioning system, J. Chem. Inf. Model. 53 (9) (2006) 1689–1699.
[33] X. Nie, Y. Lv, Y. Gong, W. Zhang, F. Li, Metal Hydride Air Conditioning of the Waste Heat of Automobile Engine Coolant Driving,” 2011 IEEE Int. Conf. Cyber Technol. Autom. Control. Intell. Syst. CYBER 2011, pp. 97–101.
[34] B. Kang, Thermal modelling and analysis of a metal hydride chiller for air conditioning, Int. J. Hydrog. Energy 20 (8) (1995) 665–674.
[35] P. Muthukumar, M. Groll, Metal hydride based heating and cooling systems: a review, Int. J. Hydrogen Energy 35 (8) (2010) 3817–3831.
[36] M. Nagel, Y. Komazaki, M. Uchida, S. Suda, Y. Matsubara, Operating characteristics of a metal hydride heat pump for generating cooled air, J. Less-Common Met. 104 (2) (1984) 307–318.
[37] C. Corgnale, B. Hardy, T. Motyka, R. Zidan, Metal hydride based thermal energy storage system requirements for high performance concentrating solar power plants, Int. J. Hydrogen Energy 41 (44) (2016) 20217–20230.
[38] D.A. Sheppard, M. Paskevicius, T.D. Humphries, M. Felderhoff, G. Capurso, J. Bellosta von Colbe, M. Dornheim, T. Klassen, P.A. Ward, J.A. Teprovich, C. Corgnale, R. Zidan, D.M. Grant, C.E. Buckley, Metal hydrides for concentrating solar thermal power energy storage, Appl. Phys. A Mater. Sci. Process. 122 (4) (2016), https://doi.org/10.1007/s00339-016-9825-0.
[39] P. Feng, L. Zhu, Y. Zhang, F. Yang, Z. Wu, Z. Zhang, Optimum output temperature setting and an improved bed structure of metal hydride hydrogen storage reactor for thermal energy storage, Int. J. Hydrogen Energy (2018) 1–13.
[40] K. Manickam, P. Mistry, G. Walker, D. Grant, C.E. Buckley, T.D. Humphries, M. Paskevicius, T. Jensen, R. Albert, K. Peinecke, M. Felderhoff, Future perspectives of thermal energy storage with metal hydrides, Int. J. Hydrogen Energy 44 (15) (2019) 7738–7745.
[41] 2009, 2009 ASHRAE Handbook: Fundementals, American Society of Heating, Refrigerating and Air-Conditioning Engineers.
[42] Office of Energy Efficiency and Renewable Energy, ‘‘Commercial and Residential Hourly Load Profiles for All TMY3 Locations in the United States,’’ OpenEI [Online]. Available: https://openei.org/doe-opendata/dataset/commercial-and-residential-hourly-load-profiles-for-all-tmy3-locations-in-the-united-states.
[43] Emerson, 2019, ‘‘Copeland Select Software.’’
[44] P. Krane, A.L. Nash, D. Ziviani, J.E. Braun, A.M. Marconnet, N. Jain, Dynamic modeling and control of a two-reactor metal hydride energy storage system, Appl. Energy. (2021).
[45] A. Tam, D. Ziviani, J.E. Braun, N. Jain, Development and evaluation of a generalized rule-based control strategy for residential ice storage systems, Energy Build. 197 (2019) 99–111.
[46] O. Comstock, 2014, Everywhere but Northeast, Fewer Homes Choose Natural Gas as Heating Fuel,’’ Today in Energy [Online]. Available: https://www.eia.gov/todayinenergy/detail.php?id=18131.
[47] National Renewable Energy Laboratory, ‘‘1991-2005 Update: Typical Meteorlogican Year 3,’’ Natl. Sol. Radiat. Database [Online]. Available: https://rredc.nrel.gov/solar/old_data/nsrdb/1991-2005/tmy3/.
[48] National Renewable Energy Laboratory, ‘‘Utility Rate Database,’’ OpenEI [Online]. Available: https://openei.org/wiki/Utility_Rate_Database.
[49] Energy Efficiency and Renewable Energy Office, 2016, ‘‘Technical Support Document: Energy Efficiency Program for Consumer Products: Residential Central Air Conditioners, Heat Pumps, and Furnaces,’’ US Dep. Energy, (December).
[50] 2017, ‘‘Argus Rare Earths Monthly Outlook,’’ Arg. Consult. Serv., (17–9).